ORIGINAL PAPER

Enhanced electrochemical performance of LiFePO$_4$ of cathode materials for lithium-ion batteries synthesized by surfactant-assisted solvothermal method

Jing Geng[1] · Shuchao Zhang[1] · Zhengguang Zou[1] · Jie Liu[1] · Shenglin Zhong[1]

Abstract

Lithium iron phosphate (LiFePO$_4$) cathode materials were synthesized by the solvothermal method with the assistance of different surfactants. The influences of polyethylene glycol 2000 (PEG 2000), polyvinylpyrrolidone (PVP), and cetyltrimethyl ammonium bromide (CTAB) on the microstructure and electrochemical performance of LiFePO$_4$ were investigated by using X-ray diffraction (XRD), scanning electron microscopy (SEM), X-ray energy dispersive spectroscopy (EDS), electrochemical impedance spectroscopy (EIS), and charge/discharge measurements. The particle size of the LiFePO$_4$ synthesized with the assistance of PEG was uniform and showed a flat rhombohedron-like shape. The initial discharge specific capacity is up to 122.80 mAh/g with an initial coulombic efficiency of 95.50% at 0.1C. LiFePO$_4$ synthesized with PVP-assisted presents a porous structure with an initial discharge specific capacity of 91.01 mAh/g. LiFePO$_4$ synthesized with CTAB-assisted shows a flower-like morphology with an initial discharge specific capacity of 100.44 mAh/g. Though the initial discharge capacities of the LiFePO$_4$ materials prepared with the assistance of CTAB and PVP are lower than those of the LiFePO$_4$ prepared without the assistance of surfactant, the two materials exhibited excellent cyclic stability at 0.1C.

Keywords Cathode materials · Solvothermal · LiFePO$_4$ · Lithium-ion battery

Introduction

Lithium-ion battery (LIB), as one of the most important energy storage technologies, has triggered a technological revolution in the past few decades. The application of LIB in portable electronic devices, including mobile phones and laptops, has greatly improved people's lives [1, 2]. However, the application of LIB in new energy vehicles has put forward higher requirements for the performance of lithium-ion batteries, which has stimulated a higher wave of research on different electrode materials and cell technologies [3, 4]. In recent years, the energy storage field is actively optimizing electrode materials and electrolyte/electrode composite interfaces to improve battery performance [5–8]. The close combination of solid electrolyte and electrode material and single ion gel polymer electrolyte crosslinked in situ has

been reported successively [9, 10]. These cleverly designed ion transport media give faster ion transport at the electrode/electrolyte interface, smaller interface impedance, and suppression of lithium dendrites. In addition, aluminum-air batteries based on copper deposition on aluminum anodes and sodium-ion batteries based on sodium-ion pre-intercalation TiO$_2$ anodes have also been developed, which has the dual advantages of performance and cost [11, 12]. However, most of the research only focuses on the design of electrolyte and anode materials; the research on the cathode material itself, for instance, based on the conductive material coating of the positive electrode material and the reasonable design of the morphology [13], which has a critical influence on performance, are rarely mentioned in recent year.

Olivine-type LiFePO$_4$ has become one of the most widely used cathode materials for power lithium-ion battery due to its stable discharge plateau, superior cyclic stability and good safety, low cost, and environmental friendliness [14, 15]. However, the lower electrical conductivity and sluggish Li$^+$ diffusivity severely limit its further development [16–18]. Recently, to improve the performance of LiFePO$_4$, people are not only committed to the later modification

Jing Geng and Chaoshu Zhang contributed equally to this work

✉ Zhengguang Zou
zouzgglut@163.com

[1] College of Materials Science and Engineering, Guilin University of Technology, Guilin, China

research, but also try to improve the performance by optimizing the synthesis process. The commonly used preparation methods of LiFePO$_4$ include high temperature solid phase method [19–21], carbothermic reduction method [22], hydrothermal/solvothermal method [23–26], sol–gel method [27, 28], co-precipitation method [29, 30], microwave treatment [31, 32], and spray thermal decomposition technology [33]. Among these methods, the solvothermal method attracts much attention because of its simple operation, intact crystal grains, and controllable morphology of the synthesized product.

Surfactant is a chemical substance that can reduce the surface tension of water or oil–water interface by adsorbing at the gas–liquid interface. When dissolved in a solution, it can often reduce the surface energy and disperse particles. It has an important impact on the morphology and size of the prepared materials, which are crucial for determining electrochemical performance [34, 35]. It has been reported that the grain size and morphology of the prepared samples can be well controlled by adding suitable surfactants in the solvothermal reaction process [36–39].

In this work, LiFePO$_4$ materials with different morphologies were synthesized by the solvothermal method with water and ethylene glycol as solvents. In particular, the effects of different surfactants (PEG 2000, PVP, and CTAB) on the structure, morphology, particle size, and electrochemical performance of the as-prepared LiFePO$_4$ were studied in detail, and the formation mechanism of the special morphology was analyzed. Compared with the LiFePO$_4$ synthesized with the assistance of PEG that has a low polymerization degree, the method used in this article reduces the amount of polyethylene glycol and simplifies the experimental operation process. The results show that the assistance of surfactants in the solvothermal process has a positive effect on optimizing the morphology and performance of LiFePO$_4$ as a cathode material for a lithium-ion battery.

Experimental

Materials synthesis

All chemicals were purchased from Xilong Scientific Co., Ltd. and were used directly without further processing. The cathode materials of LFP were synthesized via a solvothermal method by using ferrous sulfate (FeSO$_4$·7H$_2$O), lithium hydroxide (LiOH·H$_2$O), and phosphoric acid (H$_3$PO$_4$) as raw materials.

The raw materials were weighed according to the molar ratio of Li:Fe:P = 3:1:1. Typically, 0.632 g polyethylene glycol 2000 (PEG 2000), polyethylene pyrrolidone (PVP), or cetyltrimethylammonium bromide (CTAB) were dissolved in a beaker containing 20 ml of ethylene glycol (99.7%) and

10 ml of water. Then 1.112 g FeSO$_4$·7H$_2$O and 0.4612 g H$_3$PO$_4$ (85%, AR) were slowly added into the aforementioned solution in sequence; afterwards, 0.5035 g LiOH were fully dissolved in 10-ml water and added to the aforementioned solution. After stirring for 1 h, the mixed solution containing raw materials was transferred into a reactor of polytetrafluoroethylene lining with a volume of about 80 ml and kept at 180 °C for 6 h. After the reactor cooled to room temperature, the obtained precipitated products were washed and centrifuged alternately with deionized water and absolute ethanol three times. The filter cakes obtained after filtration were dried at 90 °C under vacuum and sintered under the protection of flowing high-purity nitrogen at 650 °C for 5 h with a ramp of 5 °C/min. The final products prepared with the assistance of PEG, PVP, and CTAB are named LFP-PEG, LFP-PVP, and LFP-CTAB, respectively. For comparison, LiFePO$_4$ was also prepared with the same procedure described previously but without adding any surfactant, and the final product is named LFP.

Materials characterization

The crystal structure of the as-prepared samples was characterized by X-ray diffraction. The model of the instrument is Panalytical X'Pert PRO diffractometer, using Cu Kα radiation, operating at 40 kV and 25 mA in an angular range of $10° \sim 70°$ (2θ) with a scan rate of 5° per minute. The composition of the samples was analyzed with an X-ray energy spectrometer by Oxford instrument INCA IE 350. Hitachi S-4800 field emission scanning electron microscope (FESEM) was used to observe the morphology of the as-prepared samples. The particle size and size distribution of the sample were obtained by nano-ZS from Malvern Company, UK. D50 is the particle size when the percentage of the cumulative particle size distribution of a sample reaches 50%, also called the median diameter or median particle size. D50 is used to indicate the average particle size of the powder.

Electrochemical test

The working electrode was prepared by mixing the prepared LiFePO$_4$ sample, polyvinylidene fluoride (PVDF), and acetylene black with a weight ratio of 8:1:1 in N-methyl-2 pyrrolidone (NMP) solvent. The obtained slurry was uniformly coated on an aluminum foil collector (15 μm in thickness), dried under vacuum at 120 °C for 12 h, and punched discs with a diameter of 16 mm. Coin-type cells (CR2025) were assembled in a glove box filled with high-purity argon. Commercial lithium metal foil was used as the counter electrode, Celgard 2300 membrane was used as the separator, and 1 M LiPF$_6$ in a mixture of ethylene carbonate (EC) and dimethyl carbonate (DMC) (EC/
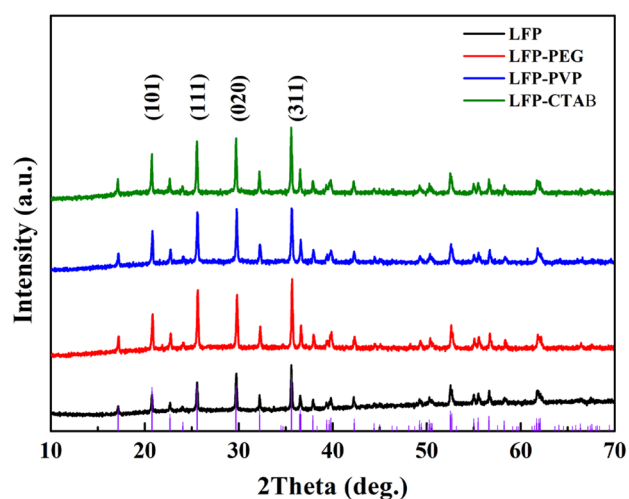
Fig. 1 XRD patterns of the sample synthesized without and with the assistance of different surfactants

DMC = 1:1 in volume) was used as the electrolyte solution. The constant current charging and discharging test of the coin cells was performed on the NEWARE CT-3008 5 V 10 mA-164 battery test system (BTS). Electrochemical impedance spectroscopy (EIS) was carried out on a CHI 860D electrochemical workstation.

Result and discussion

Figure 1a shows the XRD patterns of the LFP, LFP-PEG, LFP-PVP, and LFP-CTAB. All the diffraction peaks of the four samples can be well indexed to the standard diffraction peaks of LiFePO$_4$. The main crystal plane diffraction peaks such as (101), (111), (020), and (311) are clearly observed, indicating that all the four samples have olivine structures with orthogonal Pnma space group. The sharp and high diffraction peaks of the prepared samples suggest their high purity and good crystallinity. No other impurity peaks were observed in the XRD patterns, which indicates that the addition of PEG 2000, PVP, and CTAB during the solvothermal process has a neglectable impact on the phase structure of the prepared material. Table 1 presents

Table 1 Lattice parameters and unit cell volume for the samples synthesized without and with different surfactants
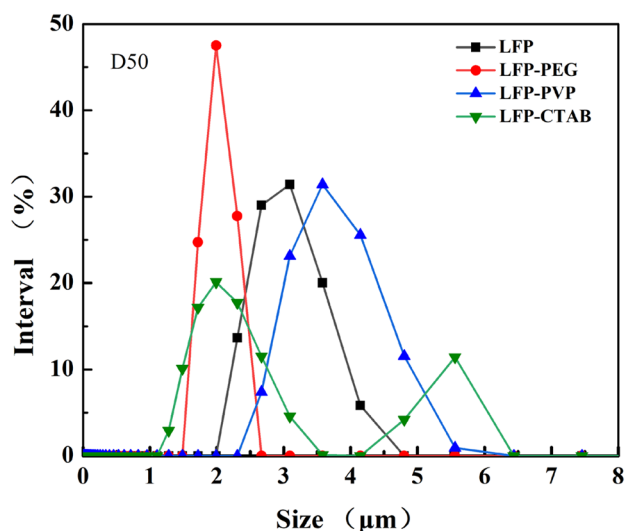
Sample name	a (Å)	b (Å)	c (Å)	V (Å^3)
LFP	10.3264	6.0044	4.6929	290.98
LFP-PEG	10.3301	6.0063	4.6943	291.33
LFP-PVP	10.3325	6.0045	4.6934	291.19
LFP-CTAB	10.3345	6.0047	4.6935	291.25

the unit cell parameters of the four samples calculated by Jade 6.0 software based on the XRD results. It can be seen that the unit cell parameters of the samples synthesized with the assistance of the surfactants increased, which is beneficial to the extraction and insertion of Li$^+$ and the improvement of cycle performance. It can be seen that the difference in unit cell parameters of the samples synthesized with and without the assistance of surfactants is very small, which further shows that the presence of surfactants does not change the phase of the material.

Figure 2a–d shows the SEM image changes of the morphology of the samples prepared with and without the assistance of surfactants. It can be seen that the addition of surfactants (PEG 2000, PVP, CTAB) has caused a significant change in the morphology of the material. The LFP sample synthesized without the assistance of surfactants shows flat rhombohedron-like morphology, and the particle size is uneven. The length of the biggest particle is about 3 μm in large diagonal, 1.5 μm in short diagonal, and about 0.5 μm in thickness. As shown in Fig. 2a, the primary particles agglomerate seriously. The LFP-PEG sample also shows flat rhombohedron-like morphology with the length of the large diagonal of about 1.5 μm, short diagonal of about 0.5 μm, and thickness of about 0.3 μm. The smaller LiFePO$_4$ particles were synthesized with the assistance of PEG 2000, with a very narrow particle size distribution. The overall dispersion of the particles also improved. This is due to the unique amphiphilic properties of PEG as a surfactant. When it dissolves in solution, the molecular chain changes from a jagged chain to a folding chain, and even further folds into other shapes, as shown in Fig. 3. The hydrophilic bridging oxygen atoms on the outside and water molecules or alcohol molecules combine with hydrogen bonds to form a hydrophilic shell. As the lipophile -CH$_2$-CH$_2$- is located within the molecular chain, this causes the PEG molecular chain in solution to align orientally and form an unusual micelle [40]. The micelles form a protective film on the surface of the LiFePO$_4$ particles, thereby preventing the growth of the particles and improving the crystallinity to some extent. In addition, the increase in the viscosity of the solution results in cations being trapped in it, which speeds up the nucleation speed of crystals and inhibits crystal growth [41, 42].

The LFP-PVP sample has flat rhombohedron particles with a porous structure. Compared with the LFP sample, it can be seen that the particle size increased significantly. The length range of the biggest particle is about 2 ~ 5 μm in large diagonal, 1 ~ 2.5 μm in short diagonal, and about 0.4 ~ 0.6 μm in thickness. It can be seen from Fig. 2c that the agglomeration between particles is obvious, and some particles even grew into irregular clusters. In addition, a large number of pores can be observed on the surface of the

Fig. 2 SEM images of the samples synthesized without and with different surfactants: (**a**) LFP, (**b**) LFP-PEG, (**c**) LFP-PVP and (**d**) LFP-CTAB

particles, indicating that the presence of PVP in the solvo-thermal process contributes to the formation of the porous structure.

The LFP-CTAB sample has a flower-like morphology with a diameter of 3~5 μm, which is assembled by single-crystal particles. The single-crystal particles show porous flat rhombohedron shape with the length of the large diagonal of 2~4 μm, short diagonal size 1~2 μm, and thickness

of about 0.5 μm. The formation of the flower-like structure may be related to the Ostwald ripening process (the smaller particles may atrophy under the action of interface energy, while the bigger particles will continue to grow up). As a surfactant, CTAB will form a large number of micelles in the solution when the concentration reaches a certain level, which will hinder the further growth of the crystals [43]. However, the supply of ions in the reaction system is

Fig. 3 Schematic diagram of the change of chain configuration of the PEG molecules in water

Fig. 4 The particle size of the samples synthesized without and with different surfactants

continuous, so the smaller crystals in the solution may dissolve and then regrow to bigger crystals. After that, bigger crystals continue to grow radially from the nucleus and break the obstacles of micelles. The secondary particles of self-assembled flower-like were formed eventually. In addition, some agglomerated and irregular substances with framework structures can also be seen in Fig. 2d, which may be related to the incomplete decomposition of CTAB [23, 44].

Figure 4 shows the particle size test results of the samples synthesized without and with the assistance of surfactants. It can be seen that the D50 value for the LFP sample is

3.091 µm and the D50 value of the sample LFP-PEG is 1.990 µm. It is obvious that the sample synthesized with the assistance of PEG 2000 has the smallest and most uniform particle size. Due to the agglomeration between particles and the growth of secondary particles, the particle size of the samples synthesized with the assistance of PVP or CTAB is generally big. In particular, the LFP-CTAB sample exhibited a bimodal phenomenon due to the big difference in particle size. This result is consistent with the result of the SEM image.

Figure 5 shows the EDS images of the four samples. It can be seen that the presence of surfactants does not introduce other impurity elements than carbon. This is because PEG, PVP, and CTAB could be completely decomposed at 400℃, 500℃, and 300℃, respectively [37, 45]. Therefore, even if a small amount of surfactants is left after the multiple washings, it will decompose to amorphous carbon during the subsequent heat treatment and finally remain in the samples. This is consistent with the result of the X-ray diffraction pattern in Fig. 1. The presence of a small amount of carbon helps to improve the electrical conductivity between particles and the electrochemical performance of the material [46, 47].

Figure 6a–d shows the charge and discharge curves of four samples in the first, fiftieth, and one-hundredth cycles measured at room temperature at 0.1C. It can be seen from the figure that each sample has an obvious charging and discharging plateau, which corresponds to the extraction and insertion of Li+ during the charging and discharging processes. The voltage plateau for the charging process is around 3.5 V, and the voltage plateau for the discharging process is around 3.4 V. The charge–discharge plateau of

Fig. 5 The EDS spectra of the samples synthesized without and with different surfactants: (**a**) LFP, (**b**) LFP-PEG, (**c**) LFP-PVP and (**d**) LFP-CTAB
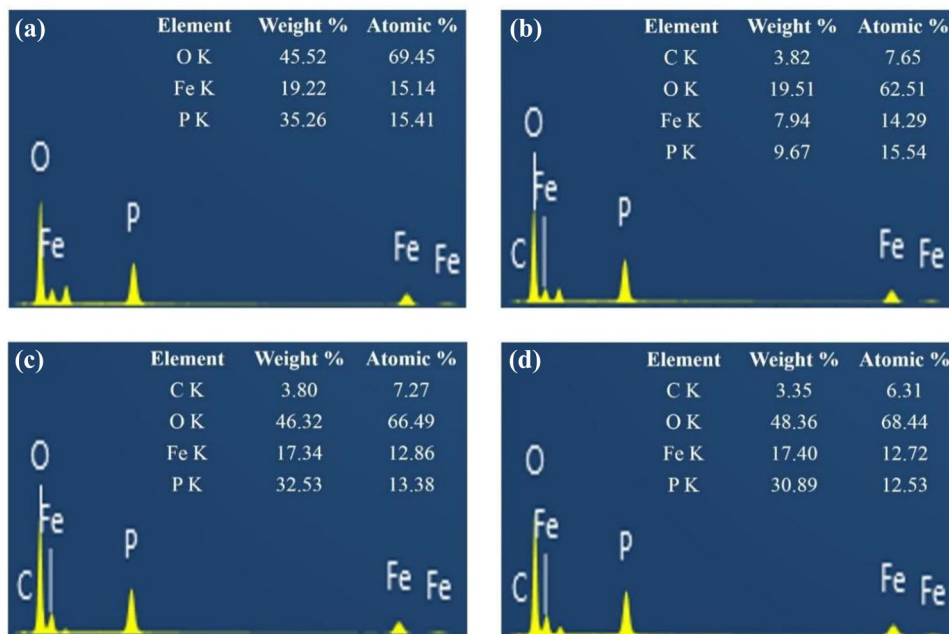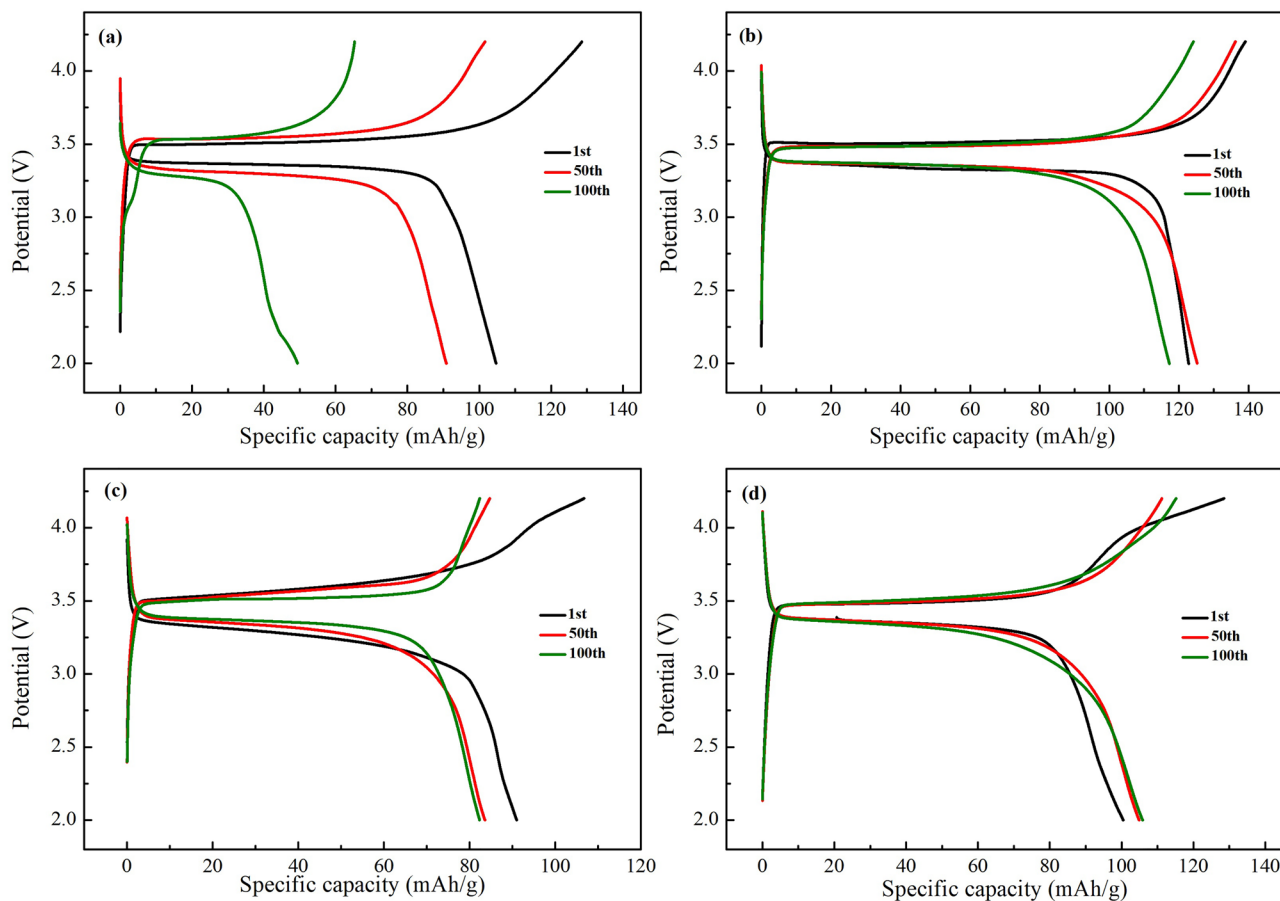
Fig. 6 The discharge/charge profiles in the first, fiftieth, and one-hundredth cycles of the samples synthesized without and with different surfactants at 0.1C in the voltage range of 2.0–4.2 V: (**a**) LFP, (**b**) LFP-PEG, (**c**) LFP-PVP and (**d**) LFP-CTAB

the samples synthesized with the assistance of surfactants is generally longer, and the charge and discharge curves at different cycles have higher coincidence degree, which indicates that the samples have better stability during the charge–discharge process. The initial charge/discharge capacities of LFP, LFP-PEG, LFP-PVP, and LFP-CTAB are 128.57/104.67 mAh/g, 139.10/122.80 mAh/g, 106.71/91.01 mAh/g, and 128.56/100.44 mAh/g, respectively. The

corresponding coulombic efficiencies are 81.41%, 88.28%, 85.30%, and 78.13%, respectively. It can be seen that the coulombic efficiencies of the samples in the first cycle are generally low. The reason may be that the structure of the material has changed after the extraction of Li$^+$ in the first cycle, resulting in the decrease of the original embeddable vacancies of Li$^+$. This leads to the fact that causing the extracted lithium ions cannot be fully inserted, resulting in a

Fig. 7 (**a**) The cycling performance and coulombic efficiency of the samples synthesized without and with different surfactants at 0.1C; (**b**) the rate performance of the four samples synthesized without and with different surfactants
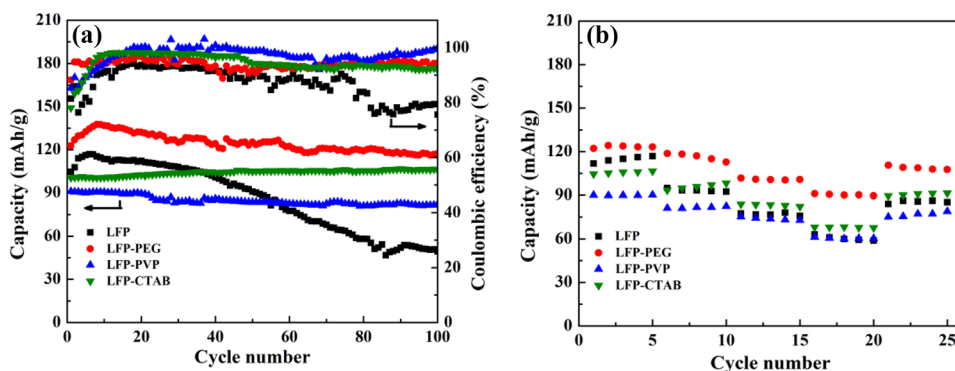
loss of capacity [48]. On the other hand, the formation of the SEI film during the first charge and discharge process will also cause the consumption of lithium ions, which increases the irreversible capacity of the first charge and discharge and reduces the coulombic efficiency of the electrode material. The sample synthesized with the assistance of PEG has the highest initial capacity, which may be due to the fact that its smaller particle size is beneficial to shortening the migration path of lithium ions and increasing the contact area between active materials and the electrolyte. This is of great benefit to improve the utilization of active materials. It can be seen that the initial capacity of the samples synthesized with the assistance of PVP or CTAB is lower than that of the samples without surfactants. This can be attributed to the big particle size and serious agglomeration, which makes it difficult for the electrolyte to penetrate the particles at the initial stage. This causes the loss of active material and the decrease of the initial specific capacity. In addition, according to the "radial model" proposed by Padhi [49], a bigger particle size will increase the diffusion path of lithium ions and hinder the progress of electrochemical reactions. This will hinder the intercalation and deintercalation of lithium ions at the center of the particle, resulting in a decrease in the initial specific capacity.

Figure 7a shows the cycling performance and coulombic efficiency of LFP, LFP-PEG, LFP-PVP, and LFP-CTAB samples at a current density of 17 mA/g (0.1C), and the voltage range is 2.0 to 4.2 V. It can be seen from Fig. 7 that the initial discharge specific capacities of the samples are 104.67 mAh/g (LFP), 122.80 mAh/g (LFP-PEG), 91.01 mAh/g (LFP-PVP), and 100.44 mAh/g (LFP-CTAB). The LFP-PEG sample has the highest initial discharge specific capacity because of its small particles and large contact area with the electrolyte, which facilitates the intercalation and deintercalation of Li$^+$ and reduces the electrode polarization during the reaction [50]. After 100 cycles, the residual discharge specific capacities of the samples are 49.41 mAh/g (LFP), 117.28 mAh/g (LFP-PEG), 82.34 mAh/g (LFP-PVP), and 105.85 mAh/g (LFP- CTAB), corresponding to the capacity retention rate of 47.21%, 95.50%, 90.47%, and 105.39%. It can be seen that all the samples synthesized with the assistance of surfactants show better cycling stability, which is mainly due to the effect of morphology adjustment of surfactants in the solvothermal reaction process. Among them, the LFP-CTAB sample has a slight increase in discharge specific capacity after cycling. The reason may be related to the special crystal structure. As the charge and discharge reaction progresses, the central part of the flower-like particles is gradually activated and participates in the electrochemical reaction to contribute to the increased capacity. In addition, according to the analysis results in Table 1, it can be observed that the volumes of the unit cell of the samples synthesized with the assistance of surfactant has increased, which is beneficial to the extraction and insertion of lithium ions and the improvement of the cycle performance of the material.

Figure 7b shows the rate performance of the LFP, LFP-PEG, LFP-PVP, and LFP-CTAB samples at the rates of 0.1, 0.2, 0.5, and 1C. It can be seen from the figure that the specific discharge capacity of the sample drops significantly with the increase of the discharge rate. This is because the time of extraction and insertion of lithium ions is shortened

Fig. 8 SEM image of the samples synthesized without and with different surfactants after cycling: (**a**) LFP, (**b**) LFP-PEG, (**c**) LFP-PVP and (**d**) LFP-CTAB
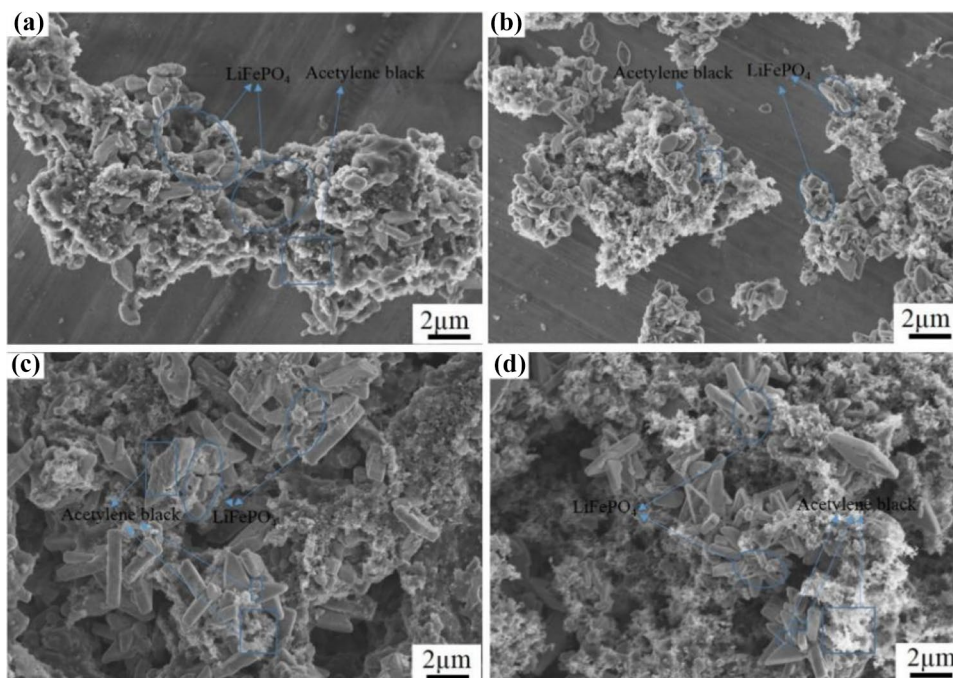
at a high current density, which makes it impossible for some lithium ions to extract and insert the crystal lattice completely. When the discharge rate drops back to 0.1C, the capacity of the LFP sample synthesized without the assistance of surfactant has increased. Nevertheless, there is still a large loss compared to its initial discharge specific capacity at 0.1C. This may be due to the rapid extraction and insertion of lithium ions at high current densities damaging the structure of the material seriously, causing some active materials to dissolve or fall off. The samples synthesized with the assistance of the different surfactants show better rate performance, which may be due to their stable morphology and structure. In particular, the sample LFP-PEG has the best rate performance. The possible reason is that the presence of PEG 2000 refines the material particles to short the diffusion path of lithium ion, which is beneficial to the rapid extraction and insertion of lithium ions in LiFePO$_4$.

In order to explore the capacity decay of the samples during the charge and discharge, we disassembled the battery after the test and characterized the morphology of the samples. Figure 8a–d shows the SEM images of the samples synthesized with and without the assistance of surfactants after 100 cycles. Compared with the morphology before cycling, some acetylene black appeared in the sample, which is added to improve the conductivity of the material during the production of the positive plate. It can be clearly seen that the morphology and structure of each sample have been damaged to varying degrees after cycling. As shown in Fig. 8a, the crystal grains of the LFP sample show severe pulverization after cycling. This reflects its poor structural stability. The destruction of the crystal structure will hinder the extraction and insertion of lithium ions in the crystal lattices, resulting in a rapid capacity decay. This further gives the reason why the sample LFP in Fig. 7 exhibits poor cyclic stability.

The LFP-PEG sample with good cyclic stability has less morphological change after cycling, as shown in Fig. 8b. Although part of the crystal grains also appeared to be damaged and powdered, the degree of damage is relatively small overall. After the cycles, the crystal grains of the LFP-PVP sample appeared fragmented, showing excellent structural stability. However, its big particle size prevents the electrolyte from completely saturating the particles and hinders the extraction and insertion of lithium ions. This leads to the inactivation of the active material at the center of the particle, resulting in a significant decrease of the initial discharge specific capacity. In addition, it can be clearly seen from Fig. 8c that lots of acetylene black have entered the pores on the crystal grain surface. On the one hand, the presence of acetylene black helps to improve the conductivity of the material. On the other hand, the fluffy acetylene black is helpful to the electrolyte to better infiltrate the material to improve the diffusion of lithium ions. It can be observed from Fig. 8d that the particles of the LFP-CTAB sample after the cycles exhibit some slight fracture, showing the best structural stability. The presence of acetylene black can also be seen in the pores at the center of the flower-like structure, which plays an extremely important role in improving the conductivity of the material and releasing the performance of the active material in the center of the flower-like structure. It is speculated that the small increase in capacity of the LFP-CTAB sample after the cycles may be closely related to this unique morphology.

Figure 9a shows the EIS plots of the samples, which are mainly composed of a depressed semi-circle in the higher frequency range and an inclined line in the lower frequency range. The diameter of the semi-circle reflects the charge transfer resistance during the electrochemical reaction, and the slope of the inclined line reflects the diffusion rate of
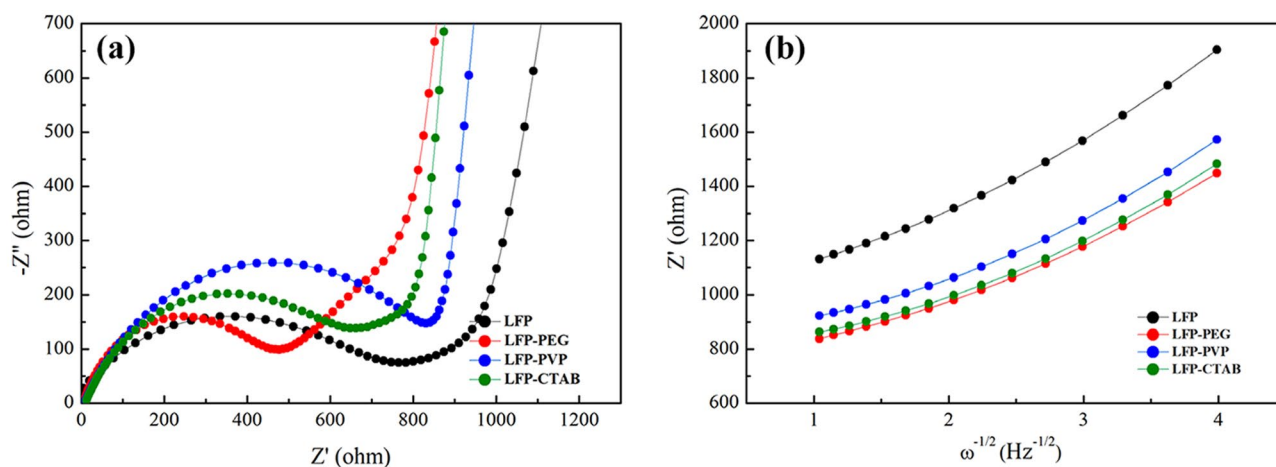
Fig. 9 (a) EIS plots of the samples synthesized without and with different surfactants; (b) Z' vs. $\omega^{-1/2}$ plots obtained from EIS measurements

lithium ions in the bulk phase of the material [51]. The figure shows the equivalent circuit of the reaction process with the electrode, where R1 represents the solution resistance, R2 represents the charge transfer resistance in the process of the electrochemical reaction, W1 represents the Warburg impedance related to lithium-ion diffusion in the solid active material, and CPE1 is constant phase element. According to the fitting results of the equivalent circuit diagram, the charge transfer resistances of the LFP, LFP-PEG, LFP-PVP, and LFP-CTAB samples are 764.48, 476.56, 830.49, and 661.38 Ω, respectively.

By comparison, it can be found that the charge transfer resistance of the sample synthesized with the assistance of PEG is the lowest. This is ascribed to the small particle size and the increase of the contact area between the active material and the electrolyte. This is also an important reason why the LFP-PEG sample has the highest initial discharge specific capacity and the best cyclic stability.

This result shows that a lower charge transfer resistance is beneficial to reduce the capacity attenuation of the material during the process of charging and discharging and improve the cyclic stability of the material. In order to research the diffusion of Li$^+$, we calculated the lithium-ion diffusion coefficient of the sample and gave the corresponding relationship diagram, as shown in Fig. 9b. Through data fitting, the Warburg coefficient (σ) of each sample can be obtained, and the corresponding diffusion coefficient of lithium ion (D_{Li}) can be calculated according to the following [52]:

$$D_{Li} = \frac{R^2 T^2}{2A^2 n^4 F^4 c^2 \sigma^2}$$

In this equation, R, T, A, F, and C correspond to the gas constant (8.314 J/(mol·K), the temperature in Kelvin (298 K), the area of electrode surface (2.01 cm^2), Faraday's constant (96,485 C/mol), and molar concentration of the lithium ions (2.33×10^{-2} mol/cm^3), respectively. The lithium-ion diffusion coefficient is inversely proportional to the Warburg factor σ ($Z' \sim \omega^{-1/2}$).

As shown in Table 2, the diffusion coefficients of the LFP, LFP-PEG, LFP-PVP, and LFP-CTAB samples are $0.25 \diamond 10^{-15}$, $0.40 \diamond 10^{-15}$, $0.36 \diamond 10^{-15}$, and $0.39 \diamond 10^{-15}$ cm^2/s, respectively. It can be seen that the diffusion coefficient of LiFePO$_4$ cathode materials synthesized with the assistance

Table 2 σ and D_{Li} values of samples synthesized without and with different surfactants

Sample designation	σ	D_{Li} (cm^2/s)
LFP	255.51	$0.25 \diamond 10^{-15}$
LFP-PEG	201.08	$0.40 \diamond 10^{-15}$
LFP-PVP	213.67	$0.36 \diamond 10^{-15}$
LFP-CTAB	204.04	$0.39 \diamond 10^{-15}$

of surfactants was improved. This result shows that the smaller particle size, uniform particle size distribution, and porous structure can improve the immersion of the electrolyte to reduce the resistance of the materials during charge and discharge, which is beneficial for the enhancement of the electrochemical performance of the material.

Conclusion

LiFePO$_4$ cathode materials with different morphologies were synthesized by a solvothermal method with the assistance of PEG 2000, PVP, and CTAB. The LiFePO$_4$ synthesized with the assistance of PEG 2000 exhibits excellent electrochemical performance. It has a high initial discharge specific capacity of 122.80 mAh/g. After 100 cycles at 0.1C and room temperature, the capacity retention rate reaches 95.50%, which is higher than that of the sample synthesized without the assistance of surfactants. In addition, the samples synthesized with the assistance of PVP and CTAB also show excellent cyclic stability but suffer from a large capacity loss in the initial cycle. Therefore, when the surfactant-assisted solvothermal method is used to synthesize LiFePO$_4$, PEG 2000 can be preferentially used as a surfactant. Different from the previous literatures which focus on exploring the influence of surfactant dosage on the electrochemical performance of LiFePO$_4$, our work focuses on the different mechanisms of action of different surfactants in the solvothermal synthesis process. This work could provide a certain reference value for future research on the morphology optimization and particle refinement of LiFePO$_4$.

References

1. Li F, Na H, Jin W, Xu X, Wang W, Gao J (2018) Facile synthesis of CoWO$_4$/RGO composites as superior anode materials for lithium-ion batteries. J Solid State Electrochem 22(9):2767–2774
2. Liu W, Yi C, Li L, Liu S, Gui Q, Ba D, Li Y, Peng D, Liu J (2021) Designing polymer-in-salt electrolyte and fully infiltrated 3D electrode for integrated solid-state lithium batteries. Angew Chem Int Ed Engl 60(23):12931–12940
3. Falco M, Simari C, Ferrara C, Nair JR, Meligrana G, Bella F, Nicotera I, Mustarelli P, Winter M, Gerbaldi C (2019) Understanding the effect of UV-induced cross-linking on the physicochemical properties of highly performing PEO/LiTFSI-based polymer electrolytes. Langmuir 35(25):8210–8219
4. Xu X, Xiong F, Meng J, An Q, Mai L (2020) Multi-electron reactions of vanadium-based nanomaterials for high-capacity lithium batteries: challenges and opportunities. Mater Today Nano 100073
5. Tang J, Wang L, You L, Chen X, Huang T, Zhou L, Geng Z, Yu A (2021) Effect of organic electrolyte on the performance of solid

electrolyte for solid-liquid hybrid lithium batteries. ACS Appl Mater Interfaces 13(2):2685–2693

6. Wang X, Liu Z, Tang Y, Chen J, Wang D, Mao Z (2021) Low temperature and rapid microwave sintering of $Na_3Zr_2Si_2PO_{12}$ solid electrolytes for Na-Ion batteries. J Power Sources 228924

7. Hao F, Liang Y, Zhang Y, Chen Z, Zhang J, Ai Q, Guo H, Fan Z, Lou J, Yao Y (2020) High-energy all-solid-state organic–lithium batteries based on ceramic electrolytes. ACS Energy Lett 6(1):201–207

8. Piana G, Bella F, Geobaldo F, Meligrana G, Gerbaldi C (2019) PEO/LAGP hybrid solid polymer electrolytes for ambient temperature lithium batteries by solvent-free, "one pot" preparation. J Energy Storage 100947

9. Bi Z, Mu S, Zhao N, Sun W, Huang W, Guo X (2021) Cathode supported solid lithium batteries enabling high energy density and stable cyclability. Energy Storage Materials 35:512–519

10. Guan X, Wu Q, Zhang X, Guo X, Li C, Xu J (2020) In-situ crosslinked single ion gel polymer electrolyte with superior performances for lithium metal batteries. Chem Eng J 122935

11. Mutlu RN, Yazıcı B (2018) Copper-deposited aluminum anode for aluminum-air battery. J Solid State Electrochem 23(2):529–541

12. Massaro A, Muñoz-García AB, Maddalena P, Bella F, Meligrana G, Gerbaldi C, Pavone M (2020) First-principles study of Na insertion at TiO_2 anatase surfaces: new hints for Na-ion battery design. Nanoscale Advances 2(7):2745–2751

13. Hu D, Su Y, Chen L, Li N, Bao L, Lu Y, Zhang Q, Wang J, Chen S, Wu F (2021) The mechanism of side reaction induced capacity fading of Ni-rich cathode materials for lithium ion batteries. J Energy Chem 58:1–8

14. Lin D, Liu Y, Cui Y (2017) Reviving the lithium metal anode for high-energy batteries. Nat Nanotechnol 12(3):194

15. Tian X, Zhou Y, Tu X, Zhang Z, Du G (2017) Well-dispersed $LiFePO_4$ nanoparticles anchored on a three-dimensional graphene aerogel as high-performance positive electrode materials for lithium-ion batteries. J Power Sources 340:40–50

16. Drezen T, Kwon NH, Bowen P, Teerlinck I, Isono M, Exnar I (2007) Effect of particle size on $LiMnPO_4$ cathodes. J Power Sources 174(2):949–953

17. Fang HS, Li LP, Li GS (2007) Hydrothermal synthesis of electrochemically active $LiMnPO_4$. Chem Lett 36(3):436–437

18. Kim TR, Kim DH, Ryu HW, Moon JH, Lee JH, Boo S, Kim J (2007) Synthesis of lithium manganese phosphate nanoparticle and its properties. J Phys Chem Solids 68(5–6):1203–1206

19. Hu Q, Lia JY, Zou BK, Yu MF, Tang ZF, Wen ZY, Chen CH (2017) Improving the rate and low-temperature performance of $LiFePO_4$ by tailoring the form of carbon coating from amorphous to graphene-like. J Solid State Electrochem 22(3):797–805

20. Ding YH, Huang GL, Li HH, Xie HM, Sun HZ, Zhang JP (2015) Double carbon nano coating of $LiFePO_4$ cathode material for high performance of lithium ion batteries. J Nanosci Nanotechnol 15(12):9630–9635

21. Zhu BQ, Li XH, Wang ZX, Guo HJ (2006) Novel synthesis of $LiFePO_4$ by aqueous precipitation and carbothermal reduction. Mater Chem Phys 98(2–3):373–376

22. Zhao J, He J, Zhou J, Guo Y, Wang T, Wu S, Xue H (2011) Facile synthesis for $LiFePO_4$ nanospheres in tridimensional porous carbon framework for lithium ion batteries. J Phys Chem C 115(6):2888–2894

23. Liang F, Yao Y, Dai Y, Yang B, Ma W, Watanabe T (2012) Preparation of porous structure $LiFePO_4/C$ composite by template method for lithium-ion batteries. Solid State Ion 214:31–36

24. Huynh LTN, Tran TTD, Nguyen HHA, Nguyen TTT, Tran VM, Grag A, Le MLP (2018) Carbon-coated $LiFePO_4$–carbon nanotube electrodes for high-rate Li-ion battery. J Solid State Electrochem 22(7):2247–2254

25. Wang F, Fang Z, Zhang Y (2016) Polyethylene glycol-induced growth of $LiFePO_4$ platelets with preferentially exposed (010) plane as a cathode material for lithium ion battery. J Electroanal Chem 775:110–115

26. Zhou N, Wang HY, Uchaker E, Zhang M, Liu SQ, Liu YN, Cao G (2013) Additive-free solvothermal synthesis and Li-ion intercalation properties of dumbbell-shaped $LiFePO_4/C$ mesocrystals. J Power Sources 239:103–110

27. Dhindsa KS, Kumar A, Nazri GA, Naik VM, Garg VK, Oliveira AC, Vaishnava PP, Zhou ZX, Naik R (2016) Enhanced electrochemical performance of $LiFePO_4/C$ nanocomposites due to in situ formation of Fe2P impurities. J Solid State Electrochem 20(8):2275–2282

28. Qiao S, Zhu L, Han E, Li L, Du C, He Y, Liu J (2020) Selection of nitrogen source and PVP-assisted sol-gel method synthesis of $LiFe_{0.65}Mn_{0.35}PO_4/C$ as cathode material for lithium ion batteries. Ionics 5405–5415

29. Jugović D, Mitrić M, Cvjetićanin N, Jančar B, Mentus S, Uskoković D (2008) Synthesis and characterization of $LiFePO_4/C$ composite obtained by sonochemical method. Solid State Ion 179(11–12):415–419

30. Wang S, Yang H, Feng L, Sun S, Guo J, Yang Y, Wei H (2013) A simple and inexpensive synthesis route for $LiFePO_4/C$ nanoparticles by co-precipitation. J Power Sources 233:43–46

31. Zhang Y, Feng H, Wu X, Wang L, Zhang A, Xia T, Liu M (2009) One-step microwave synthesis and characterization of carbon-modified nanocrystalline $LiFePO_4$. Electrochim Acta 54(11):206–3210

32. Naik A, Zhou J, Gao C, Wang L (2014) Microwave assisted solid state synthesis of $LiFePO_4/C$ using two different carbon sources. Int J Electrochem Sci 9:6124–6133

33. Yang X, Tu J, Lei M, Zuo Z, Wu B, Zhou H (2016) Selection of carbon sources for enhancing 3D conductivity in the secondary structure of $LiFePO_4/C$ cathode. Electrochim Acta 193:206–215

34. Meligrana G, Gerbaldi C, Tuel A, Bodoardo S, Penazzi N (2006) Hydrothermal synthesis of high surface $LiFePO_4$ powders as cathode for Li-ion cells. J Power Sources 160(1):516–522

35. Oh SW, Myung ST, Bang HJ, Yoon CS, Amine K, Sun YK (2009) Nanoporous structured $LiFePO_4$ with spherical microscale particles having high volumetric capacity for lithium batteries. Electrochem Solid State Lett 12(9):A181

36. Guo J, Yu M, Wu F (2020) Preparation of high purity iron phosphate based on the advanced liquid-phase precipitation method and its enhanced properties. J Solid State Chem 121346

37. Wang B, Xu B, Liu T, Liu P, Guo C, Wang S, Zhao XS (2014) Mesoporous carbon-coated $LiFePO_4$ nanocrystals co-modified with graphene and Mg^{2+} doping as superior cathode materials for lithium ion batteries. Nanoscale 6(2):986–995

38. Qiu S, Zhang X, Li Y, Sun T, Wang C, Qin C (2017) Enhanced electrochemical performances of $LiFePO_4$-C synthesized with PEG as the grain growth inhibitor for Li-ion capacitors in $LiNO_3$ aqueous electrolyte. Pigment Resin Technol 46(1):31-39

39. Di Lupo F, Meligrana G, Gerbaldi C, Bodoardo S, Penazzi N (2015) Surfactant-assisted mild solvothermal synthesis of nanostructured $LiFePO_4/C$ cathodes evidencing ultrafast rate capability. Electrochim Acta 156:188–198

40. Bodoardo S, Gerbaldi C, Meligrana G, Tuel A, Enzo S, Penazzi N (2009) Optimisation of some parameters for the preparation of nanostructured $LiFePO_4/C$ cathode. Ionics 15(1):19

41. Tajimi S, Ikeda Y, Uematsu K, Toda K, Sato M (2004) Enhanced electrochemical performance of $LiFePO_4$ prepared by hydrothermal reaction. Solid State Ion 175(1–4):287–290

42. Recham N, Dupont L, Courty M, Djellab K, Larcher D, Armand M, Tarascon JM (2009) Ionothermal synthesis of tailor-made $LiFePO_4$ powders for Li-ion battery applications. Chem Mater 21(6):1096–1107

43. Liu G, Zhang S, Wei X, Wang S, Yu Y (2016) Controllable fabrication of LiFePO$_4$ cathode materials with multiple morphologies for lithium ion batteries. Int J Electrochem Sci 11(8):6799–6807

44. Choi D, Kumta PN (2007) Surfactant based sol–gel approach to nanostructured LiFePO$_4$ for high rate Li-ion batteries. J Power Sources 163(2):1064–1069

45. Fan M, Liang Y, Zhou F, Liu W (2012) Dramatically improved friction reduction and wear resistance by in situ formed ionic liquids. RSC Adv 2(17):6824–6830

46. Pang J, John VT, Loy DA, Yang Z, Lu Y (2005) Hierarchical mesoporous carbon/silica nanocomposites from phenyl-bridged organosilane. Adv Mater 17(6):704–707

47. Xu Z, Xu L, Lai Q, Ji X (2007) A PEG assisted sol–gel synthesis of LiFePO$_4$ as cathodic material for lithium ion cells. Mater Res Bull 42(5):883–891

48. Andersson AS, Thomas JO (2001) The source of first-cycle capacity loss in LiFePO$_4$. J Power Sources 97:498–502

49. Padhi AK, Nanjundaswamy KS, Goodenough JB (1997) Phospho-olivines as positive-electrode materials for rechargeable lithium batteries. J Electrochem Soc 144(4):1188

50. Liu A, Ma F, Chen Y (2017) Synthesis of shape-controlled Fe$_5$(PO$_4$)$_4$(OH)$_3$·2H$_2$O microcrystal via one-step hydrothermal method. Micro & Nano Letters 12(5):325–328

51. Ni S, Lv X, Ma J, Yang X, Zhang L (2014) Electrochemical characteristics of lithium vanadate, Li3VO4 as a new sort of anode material for Li-ion batteries. J Power Sources 248:122–129

52. Li X, Shao Z, Liu K, Zhao Q, Liu G, Xu B (2018) A facile ultrasound assisted high temperature ball milling synthesis of LiFePO$_4$/graphene with enhanced electrochemical performance. Int J Hydrogen Energy 43(41):18773–18782